Solid State Communications 253 (2017) 46–50

Contents lists available at ScienceDirect

Solid State Communications

journal homepage: www.elsevier.com/locate/ssc

Communication

The success of Fermi gas model for overall scaling of 2D metal-to-insulator transition data

M.V. Cheremisin

A.F.Ioffe Physical-Technical Institute, 194021 St.Petersburg, Russia

ARTICLE INFO

Keywords:
Wigner cristal
Metal to insulator transition

ABSTRACT

The melting condition for two-dimensional Wigner solid (Platzman and Fukuyama, 1974) [14] is shown to contain an error of a factor of π. The analysis of experimental data for apparent 2D metal-to-insulator transition shows that the Wigner solidification (Tanatar and Ceperley, 1989) [16] has been never achieved. Within routine Fermi gas model both the metallic and insulating behavior of different 2D system for actual range of carrier densities and temperatures is explained.

1. Introduction

Recently, much interest has been focused on the anomalous transport behavior of a wide variety of low density two-dimensional (2D) systems. It has been found that below some critical density, cooling causes an increase in resistivity, whereas in the opposite, high-density case, the resistivity decreases. The apparent metal to insulator transition was observed in n-Si MOSFET [1,2], p-GaAs [3–7], *n*-GaAs [8], *n*-SiGe [9,10] and p-SiGe [11,12] 2D systems being the subject of the recent overview [13].

2. Wigner solidification vs experiment

Let us provide the rigorous analysis of the experimental data regarding Fermi gas vs Wigner solid transition. According to Ref. [14], the melting diagram of 2D Wigner solid obeys the condition $\Gamma = E_{ee}/\langle K\rangle$, where Γ is the coefficient assumed to be a constant at the phase transition, $E_{ee} = \frac{e^2}{\epsilon}\sqrt{\pi N}$ is the Coulomb energy associated to neighboring pair of electrons, N is the 2D density. Within conventional Fermi gas model, $\langle K\rangle = kT\frac{F_1(1/\xi)}{F_0(1/\xi)}$ is the average kinetic energy of single electron, where $F_n(z)$ is the Fermi integral of the order of n, $\xi = kT/\mu$ the dimensionless temperature, μ is the Fermi energy. The average kinetic energy coincides with the thermal energy kT for classical Boltzmann carriers $|\xi|\gg 1$. In contrast, $\langle K\rangle = \mu/2$ for degenerate case $\xi \ll 1$. The solidification of strongly degenerated carriers is believed [14] to occur at certain value of the Coulomb to Fermi energy ratio $r_s = E_{ee}/\mu$. Therefore, we conclude that $r_s = \Gamma/2$. In Refs. [14,15], this ratio has been estimated as $r_s = \Gamma\frac{\sqrt{\pi}}{2}$, thus provides an extra factor $\sqrt{\pi}$ regarding Wigner crystal solidification scenario. For low-disorder 2D system Wigner solid was claimed [16] to exist at $r_s \geq 37 \pm 5$.

Following Ref. [14], the phase transition can be parameterized as it follows:

$$\frac{T}{T_c} = \frac{F_0^3(1/\xi)}{2F_1^2(1/\xi)}, \quad \frac{N}{N_c} = \frac{F_0^4(1/\xi)}{4F_1^2(1/\xi)}. \tag{1}$$

In general, the dimensional temperature $T_c = 4Ry\frac{g_v}{\Gamma^2}$ and 2D density $N_c = \frac{4}{\pi a_B^2}\frac{g_v^2}{\Gamma^2}$ contain the valley splitting factor g_v. Then $a_B = \frac{\epsilon\hbar^2}{me^2}$ and $Ry = \frac{me^4}{2\epsilon^2\hbar^2}$ is the effective Borh radius and Rydberg energy respectively, m is the effective mass. Note that for certain value of r_s the correct values T_c, $N_c \sim \Gamma^{-2}$ are smaller compared with those predicted in Refs. [14,15] by a factor of π. Actually, the Wigner diagram in terms T-N shrinks by order of magnitude. For real 2D systems the Wigner solid transition parameters are generalized in Table 1. In Fig. 1 we plot the melting curve [14] specified by Eq. (1) and, moreover, the observed range of 2D densities and temperatures reported in experiment [1–6,8–10]. Evidently, the regime of Wigner solidification remains unaffected. Consequently, we further use the conventional Fermi gas formalism to describe the properties of 2D systems.

3. Model of apparent metal-to insulator transition

At first, we represent in Fig. 2 the transport measurements setup and the band diagram for typical gated 2D system based on Si-MOSFET. The sample is placed in a chamber with the mean temperature T_0. For low-current mode the source-to-drain voltage swing U_{sd} allows one to find 2D layer resistivity which, in turn, depends on the applied gate voltage U_g. For strong inversion regime shown in Fig. 2, b the applied gate voltage results in shift of Fermi level of 2D system with respect to that of the metal gate. The carrier density is given by the number of occupied states below Fermi level counted from the bottom of the lowest subband E_0 of triangular quantum well. In thermodynamic equilibrium the applied gate voltage is given by the sum of electrostatic potential of gate-to-channel capacitor and reduced chemical potential of 2D system μ/e and, finally, the flat-band potential

http://dx.doi.org/10.1016/j.ssc.2017.01.027
Received 17 August 2016; Received in revised form 18 January 2017; Accepted 28 January 2017
Available online 31 January 2017

Table 1
The density N_c and temperature T_c of Wigner phase transition at $r_s = 42$ for different 2D systems.

2D system	ε	m/m_0	g_v	$N_c \cdot 10^{10}\text{cm}^{-2}$	T_c,K	Experiment
Si-MOSFET	7.7	0.19	2	4.9	0.6	[1,2]
p-GaAs	13	0.38	1	0.55	0.2	[3,5]
n-GaAs	13	0.068	1	0.02	0.04	[8]
n-SiGe	11.7	0.19	2	2.12	0.25	[9]

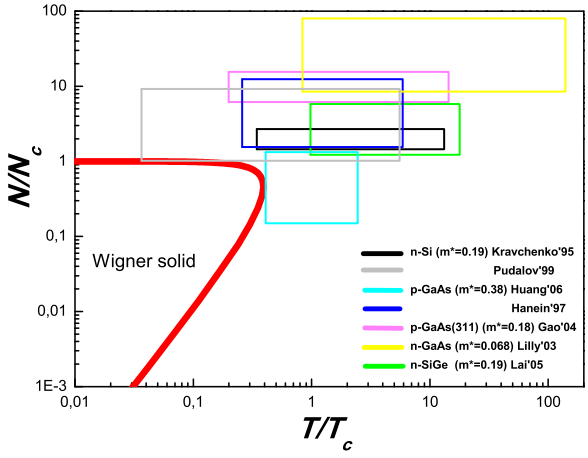

Fig. 1. (Color online)The diagram of Fermi gas to Wigner solid transition [14] according to Eq. (1) at $r_s = \frac{\Gamma}{2} = 42$ [16]. The color rectangular figures correspond to density and temperature range of apparent metal-to insulator transition in Si-MOSFET [1,2]; p-GaAs [3,5,6]; *n*-GaAs [8] and *n*-SiGe [9,10] 2D systems, modified wit respect to dimensional density N_c and temperature T_c depicted in Table 1.

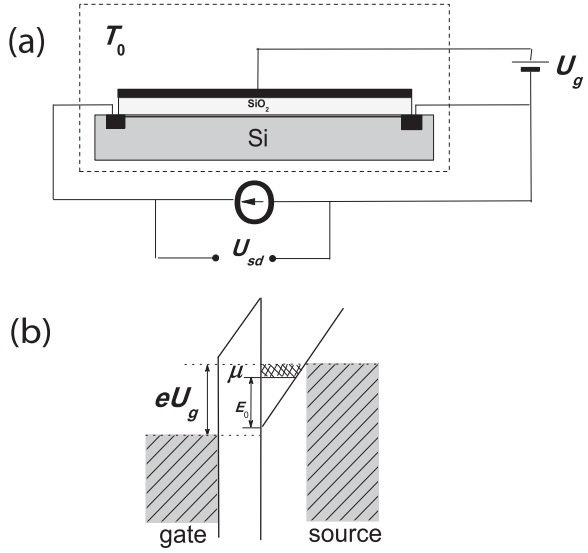

Fig. 2. a) The transport measurements setup. b) The band diagram of the of Si-MOSFET.

$U_t = \Delta W/e$. Here, ΔW is the constant difference of the work functions related to bulk silicon and metal gate respectively. The gate voltage U_g, shifted with respect to flat-band potential U_t yields

$$U_g = Q/C_g + \mu/e, \tag{2}$$

where $Q = eN$ and $C_g = \epsilon/d$ is the charge density and geometrical capacity respectively. Then, ϵ is the permittivity and d is the thickness of the dielectric layer. We argue that the applied gate voltage maintains the chemical potential of 2D system as a constant. Indeed, according to Eq. (2) the increase(decrease) of the gate voltage results in change of the chemical potential and, *in turn*, in varying of 2D carrier density. One can easily demonstrate that for typical sample geometry the second term in Eq. (2) can be ignored for strongly degenerated carriers $\xi \ll 1$, thus results in apparent evidence for 2D density changed by the gate voltage. In contrast, for non-degenerated carriers as well as for negative Fermi energies $|\xi| \gg 1$ both terms in the right side of Eq. (2) have to be accounted. These arguments provide the evidence of Gibbs statistics justified for actual 2D system.

In Ref. [17] the transport of dilute 2D systems has been analyzed taking into account both the carrier degeneracy and so-called thermal correction [18] owing to Peltier and Seebeck thermoelectric effects combined. For standard ohmic measurements the small applied current causes the heating(cooling) at the first(second) sample contact due to the Peltier effect. Under adiabatic conditions the temperature gradient is linear in current, the contact temperatures are different. The measured voltage consists of the ohmic term and, moreover, includes Peltier effect-induced thermoemf which is linear in current. The total measured resistivity [17,18].

$$\rho_{tot} = \rho(1 + \alpha^2/L) \tag{3}$$

obeys a universal features being independent on 2D carrier type. Here, $\rho = \frac{m}{Ne^2\tau}$ is the ohmic resistivity, α is 2D thermopower, $L = \frac{\pi^2 k^2}{3e^2}$ is the Lorentz number. For simplicity, we assume the energy-independent momentum relaxation time τ. With the help of Gibbs statistics 2D carrier density reads $N = N_0 \xi F_0(1/\xi)$, where $N_0 = \frac{g_v m\mu}{\pi\hbar^2}$ is the density of strongly degenerated electrons. Then, within Boltzman equation formalism the 2DEG thermopower yields $\alpha = -\frac{k}{e}\left[\frac{2F_1(1/\xi)}{F_0(1/\xi)} - \frac{1}{\xi}\right]$.

The result of theory provided by Eq. (3) and, moreover, the typical experimental data [3] for apparent 2D metal-to-insulator transition are shown in Fig. 3. We are interested first in the case of Fermi level lying above the bottom of the lowest subband which corresponds to portion of data below green separatrix($\mu = 0$). One can distinguish the puzzling temperature behavior of the resistivity as $\frac{\partial\rho}{\partial T} > 0$ for degenerated carriers $\xi \ll 1$ and $\frac{\partial\rho}{\partial T} < 0$ for high-T case $\xi \geq 1$. At fixed Fermi energy the dependence $\rho_{tot}(T)$ exhibits the maximum $\rho_m = 1.5\rho_0$ at $T_m = 0.78T_F$, where $T_F = \mu/k$ is the Fermi temperature. These values are close to those usually observed in experiment. The total resistivity specified by Eq. (3) obeys the low(high)-T asymptotes

$$\xi \ll 1, \quad \rho_{tot} = \rho_0(1 + \pi^2\xi^2/3), \tag{4}$$

$$\xi \geq 1, \quad \rho_{tot} = \rho_0 \frac{1 + \alpha_s^2/L}{1/2 + \iota + \xi \ln 2} \tag{5}$$

shown by dashed(doted) red lines in Fig. 3a. Here, $\rho_0 = \frac{h}{e^2}|k_F l|^{-1}$ is the ohmic resistivity at $T \to 0$, $k_F = \sqrt{2m|\mu|}/\hbar$ is the Fermi vector, $l_p = \hbar k_F \tau/m$ is the mean free path. Then, $\alpha_s = -\frac{k}{e}\frac{\pi^2}{6\ln 2}$ is the thermopower for non-generated carriers $\xi \gg 1$, $\iota = \frac{\alpha_s^2/L - 1}{\alpha_s^2/L + 1}$ is a correction.

Let us examine in details the behavior of 2D resistivity, namely whether the maxima positions of the resistivity curves obey the predicted relationship $\rho_m \sim 1/T_m$. To confirm this, we re-plot Fig. 4, a in terms of inverse total resistivity ρ_{tot}^{-1} vs temperature and, moreover, reproduce the experimental data reported in Ref. [5]. Surprisingly, both the theory and experiment follow the expected linear dependence $\rho_m^{-1} \sim T_m$. We check this finding for data in Fig. 3b, insert as well. As a

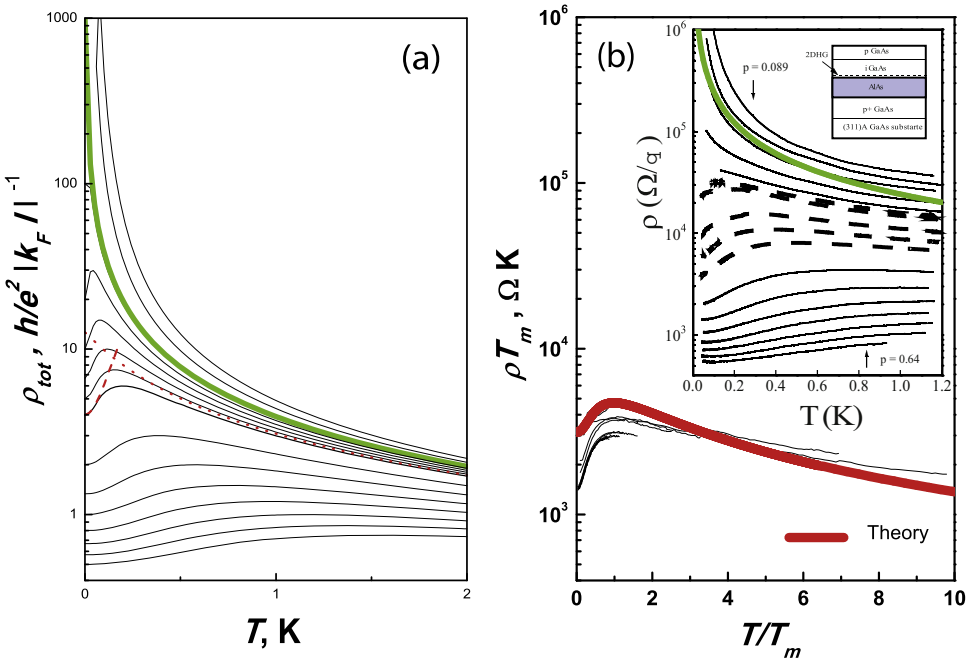

Fig. 3. (Color online) a) Temperature dependence of 2DEG resistivity, given by Eq. (3) for T_F[K] 2 - 0.25 (step 0.25), 0.2-0.05(step 0.05), 0(green line), −0.1,−0.2 at fixed value of the disorder strength: $k_F l = 1$ at $T_F = 1$ K. Dashed(doted) red line depicts the asymptote specified by Eqs. (4), (5) for degenerated $\xi \ll 1$ and non-degenerated $\xi > 1$ gas respectively at fixed $T_F = 0.25$ K. b) Experimental data(insert) for p-GaAs system after Ref. [3] for carrier density $p =$ 0.089, 0.094, 0.099, 0.109, 0.119, 0.125, 0.13, 0.15, 0.17, 0.19, 0.25, 0.32, 0.38, 0.45, 0.51, 0.57 and 0.64×10^{11} cm $^{-2}$. The add-on green line represents the result of calculation for resistivity at $\mu = 0$. Main panel: the scaling ansatz for resistivity curves(see insert), whose shapes demonstrate the maxima for certain temperature within the range $0.12 < T_m < 1.64$ K. Bold red line depicts the universal dependence $w(T/T_m)$ specified by theory.

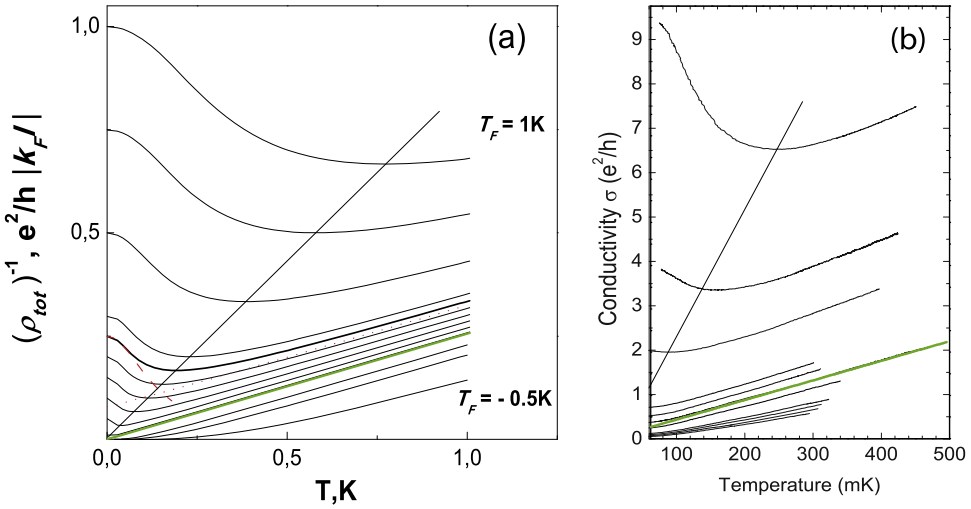

Fig. 4. (Color online) a) The inverse resistivity ρ_{tot}^{-1} vs temperature re-plotted from Fig. 3, a. Straight line depicts the minima position. b) Experimental data $\rho_{tot}^{-1}(T)$ for p-GaAs system after Ref. [5] for 2D hole density 0.8, 1.2, 1.6, 1.8, 2.5, 3.0, 3.4, 3.8, 5.1, 6.1, 7.1×10^9 cm^{-2}. In both plots the green straight line depicts the expected dependence $\rho_{tot}^{-1}(T)$ for $\mu = 0$.

result, we suggest a simple scaling procedure for apparent 2D metal-to-insulator transition data. We argue that for certain resistivity curve exhibiting a certain maximum at T_m one can find the product $\rho_{tot} T_m$ which could be a universal function of ratio T/T_m. As an example, in Fig. 3, b we represent the data [3] scaled by this manner. Remarkably, the original two-order of magnitude range resistivity data shown in Fig. 3b, insert collapse into a unique curve. Let us put on the same plot the result provided by our theory. For hole density $p = 0.64 \times 10^{11}$ cm^{-2} reported in Ref. [3] the extrapolation $T \to 0$ gives the resistivity $\rho_0 = 530\Omega$. The respective carrier mobility $\mu_p = 1.85 \times 10^5$ cm^2/Vs gives the Dingle temperature $T_D = \frac{\hbar}{k\tau} = 0.19$ K. Finally, in Fig. 3, b we put the dimensional dependence of the product $\rho_{tot} T_m = \frac{h}{e^2} \frac{T_D}{2 \cdot 0.78} w(T/T_m)$, where $w(\xi) = \frac{1+\alpha^2 / L}{\xi F_0(1/\xi)}$ is the universal function derived from Eq. (3). Data scaling result agrees with that provided by theory.

We now check the robustness of our model based on another scaling procedure made of use in Ref. [19]. It was argued that 2D resistivity obeys a certain universality being represented as dimensionless ratio $\frac{\rho_{tot} - \rho_0}{\rho_m - \rho_0}$ vs reduced temperature T/T_m. Indeed, within our notations the above ratio is equal to $2(w(T/T_m) - 1)$, thus support

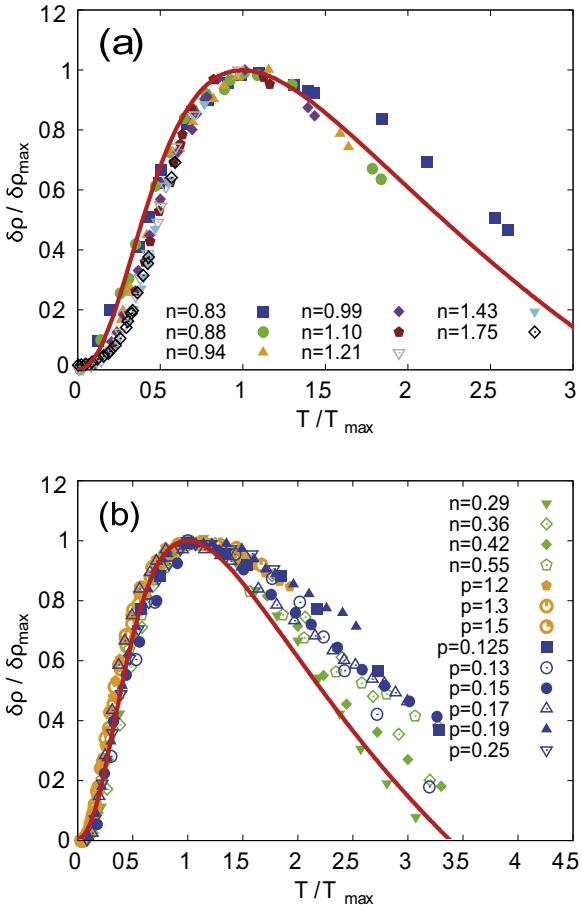

Fig. 5. (Color online) Scaling anzatz of 2D resistivity data after Ref. [19] for: a) Si-MOSFET [2] b) p-GaAs/AlGaAs(black symbols) [3], *n*-GaAs/AlGaAs(green symbols) [8], p-GaAs(orange) [20]. The the red line represents the universal function $2(w-1)$ discussed in text.

Table 2
Temperature coefficient $\mathcal{B}$.

2D system	μ, m^2/Vs	T_D,K	$\mathcal{B}$, $\frac{e^2}{h}K^{-1}$ (exp/th)	Ref
Si-MOSFET	19	0.38	2.7/0.4	[10]
p-GaAs	28	0.13	4.0/3.0	[21]
p-GaAs	32	0.11	4.7/4.5	[4,5]

universality features. Fig. 5 demonstrate the impressive agreement between the data scaling [19] and the result provided by our theory for different 2D systems.

Further progress in verifying whether our model is correct concerns the high-T dependence of the resistivity. Inverting Eq. (5) we obtain the linear dependence of inverse total resistivity $\rho_{tot}^{-1}(T)$ as it follows

$$\rho_{tot}^{-1} = \mathcal{A} + \mathcal{B}\cdot T,\ \mathcal{A} = \frac{\sigma_0(1/2+\iota)}{1+\alpha_s^2/L},\quad \mathcal{B} = \frac{e^2}{h}\frac{1}{T_D}\frac{2g_v\ln 2}{1+\alpha_s^2/L}. \tag{6}$$

Here, $\sigma_0 = 1/\rho_0$ is 2D conductivity at zero temperature. High-T linear behavior of inverse total resistivity is clearly seen in experiment (see Fig. 4, b) and, therefore, available for qualitative analysis with respect to theory. The estimates for temperature coefficient $\mathcal{B}$ are summarized in Table 2 being in agreement with theory predictions. Note that zero Fermi energy case $\mu = 0$ (see green lines in Fig. 4) is of special interest since the inverse total resistivity $\rho_{tot}^{-1} = \mathcal{B}\cdot T$ vanishes at $T \to 0$. In contrast, the resistivity strongly increases as $1/T$ at $T \to 0$ shown by the green line in both panels of Fig. 3.

Finally, we consider the most intriguing case of Fermi level laying below the bottom of the conducting band, i.e. when $\xi < 0$. This regime corresponds to portion of data below $\mu = 0$ seperatix in Fig. 4. For actual strong insulating case $|\xi| \ll 1$ the 2D density is exponentially small $\sim|\xi|\exp(-1/|\xi|)$, while the the thermopower behavior yields the Boltzman form $\alpha \sim \frac{k}{e}\frac{1}{\xi}$. Finally, we obtain the asymptote for 2D resistivity as it follows

$$\xi < 0,\ |\xi| \ll 1,\quad \rho_{tot} = \rho_0\frac{3}{\pi^2}|\xi|^{-3}\exp(1/|\xi|) \tag{7}$$

In order to compare our results with experimental data, in Fig. 6a we present the log-log version of Fig. 4a. The curves demonstrate the progressive change from high-T linear trend to low-T activated behavior. As expected, low-T activated behavior is described by inverted Eq. (7). Surprisingly, the experimental data [4] shown in Fig. 6b demonstrate a similar behavior. Note that there exists an overall failure [4] to fit low-T data(see in Fig. 6b) within conventional variable range hopping formalism $\rho_{tot}^{-1} \sim e^{(-T^*/T)^\nu}$, where $\nu = 1/3$ and $\nu = 1/2$ corresponds to Mott [22] and Efros-Shklovskii [23] predictions respectively.

Finally, we confirm validity of our results regarding up-to-date measurements made of use by lock-in technique. The main advantage of the selective detection technique with respect to conventional ac method concerns the possible measurements at small signal to noise ratio. Following Ref. [18], the ac measurements lead to resistivity correction as well. Moreover, apart from active component of the correction there exists also a reactive component. Remarkably, the total resistivity specified by Eq. (3) remains unchanged [18] below critical frequency $f_{cr} = D/l^2$ dependent on thermal inertial effects. Here, l is the sample length related to ac source inputs. Then, D is the thermal diffusion coefficient which can be estimated as electron(hole) diffusion coefficient as it follows

$$D = \frac{\sigma}{e^2}\left(\frac{dn}{d\mu}\right)^{-1}. \tag{8}$$

For non-degenerated carriers $\mu \ll kT$ Eq. (8) provides Einstein relationship $D = \frac{\mu_{p,e}}{e}kT$, while in the opposite case of degenerated carriers one obtains $D = \frac{\mu_{p,e}}{e}\mu$. As an example, we estimate Fermi temperature $T_F = 4.6\ \mathrm{K} \gg T$ for certain metallic curve($p = 0.64\times10^{11}\ \mathrm{cm}^{-2}$ data in Ref. [3]) shown in Fig. 3, b. For actual hole mobility $\mu_p = 1.85\times10^5$ cm^2/Vs and typical sample length $l \sim 5$ mm [1] we obtain the critical frequency as $f_{cr} = 290$ Hz. Even for non-degenerated holes at lowest temperatures $T \sim 50$ mK we obtain the critical frequency ~3 Hz, which is comparable with that used in actual lock-in measurements. We emphasize that spectral analysis of both the active and reactive components of the measured resistivity could eliminate the role of thermoelectric effects.

In conclusion, we demonstrate that Wigner solidification has been never achieved in experiments dealt with apparent metal to insulator transition. The observed anomalies of 2D transport behavior is explained within conventional Fermi gas formalism invoking the important correction to measured resistivity caused by Peltier and Seebeck effects combined. We represent the experimental evidence confirming the solidity and universality of the above model.

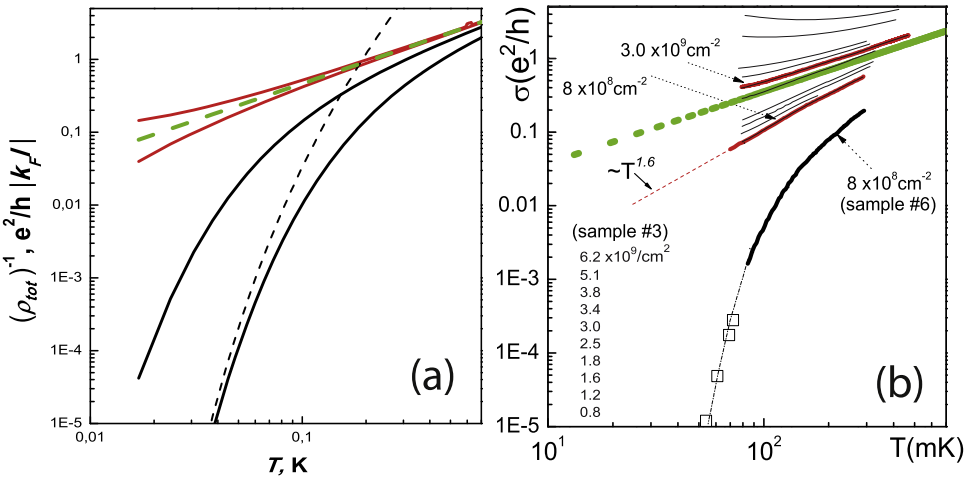

Fig. 6. (Color online) a) The temperature dependence of inverse total resistivity ρ_{tot}^{-1} for different values of the Fermi temperature $T_F[K] = 0.01; -0.01; -0.1; -0.3$ and fixed Dingle temperature $T_D = 0.11$ K. The dashed green line corresponds to $T_F = 0$. The dotted line represents the asymptote specified by Eq. (7). b) Re-plot of experimental data after Refs. [4,5] shown in Fig. 4 b, for p-GaAs sample($T_D = 0.11$ K, see Table 1) for hole density 6.2, 5.1, 3.8, 3.4, 3.0, 2.5, 1.8, 1.6, 1.2, 0.8 × 10^9 cm^{-2}. The dotted green line corresponds to zero Fermi energy. The bold black line depicts the insulating behavior of high-disordered sample studied in Ref. [4].

References

[1] S.V. Kravchenko, Whitney E. Mason, G.E. Bowker, J.E. Furneaux, V.M. Pudalov, M. D'Iorio, Phys. Rev. B. 51 (1995) 7038.
[2] V.M. Pudalov, G. Brunthaler, A. Prinz, G. Bauer, Phys. Rev. B. 60 (1999) R2154.
[3] Y. Hanein, U. Meirav, D. Shahar, C.C. Li, D.C. Tsui, Hadas Shtrikman, Phys. Rev. Lett. 80 (1998) 1288.
[4] Jian Huang, D.S. Novikov, D.C. Tsui, L.N. Pfeiffer, K.W. West, Phys. Rev. B. 74 (2006) 201302 (R).
[5] Jian Huang, L.N. Pfeiffer, K.W. West, Phys. Rev. B. 83 (2011) 081310 (R).
[6] X.P.A. Gao, G.S. Boebinger, A.P. Mills, A.P. Ramirez Jr., L.N. Pfeiffer, K.W. West, Phys. Rev. Lett. 93 (2004) 256402.
[7] R.L.J. Qiu, X.P.A. Gao, L.N. Pfeiffer, K.W. West, Phys. Rev. B. 83 (2011) 193301; R.L.J. Qiu, X.P.A. Gao, L.N. Pfeiffer, K.W. West, Phys. Rev. Lett. 108 (2012) 106404.
[8] M.P. Lilly, J.L. Reno, J.A. Simmons, I.B. Spielman, J.P. Eisenstein, L.N. Pfeiffer, K.W. West, E.H. Hwang, S. Das Sarma, Phys. Rev. Lett. 90 (2003) 056806.
[9] K. Lai, W. Pan, D.C. Tsui, S.A. Lyon, M. Muhlberger, F. Schaffler, Phys. Rev. B. 72 (2005) 081313 (R).
[10] K. Lai, W. Pan, D.C. Tsui, S. Lyon, M. Muhlberger, F. Schaffler, Phys. Rev. B. 75 (2007) 033314.
[11] P.T. Coleridge, R.L. Williams, Y. Feng, P. Zawadzki, Phys. Rev. B. 56 (1997) 12764 (R).
[12] V. Senz, U. Doetsch, U. Gennser, T. Ihn, T. Heinzel, K. Ensslin, R. Hartmann, D. Gruetzmacher, Ann. Phys. 8 (1999) 237.
[13] B. Spivak, S.V. Kravchenko, S.A. Kivelson, X.P.A. Gao, Rev. Mod. Phys. 82 (2010) 1743.
[14] P.M. Platzman, H. Fukuyama, Phys. Rev. B. 10 (1974) 3150.
[15] T. Ando, A.B. Fowler, F. Stern, Rev. Mod. Phys. 54 (1982) 437.
[16] B. Tanatar, D.M. Ceperley, Phys. Rev. B. 39 (1989) 5005.
[17] M.V. Cheremisin, Physica E 27 (2005) 151.
[18] C.G.M. Kirby, M.J. Laubitz, Metrologia 9 (1973) 103.
[19] M.M. Radonjic, D. Tanaskovic, V. Dobrosavljevic, K. Haule, G. Kotliar, Phys. Rev. B. 85 (2012) 085133.
[20] X.P.A. Gao, G.S. Boebinger, A.P. Mills Jr, A.P. Ramirez, L.N. Pfeiffer, K.W. West, Phys. Rev. Lett. 94 (2005) 086402.
[21] X.P.A. Gao, A.P. Mills Jr., A.P. Ramirez, L.N. Pfeiffer, K.W. West, Arxiv:cond-mat/0308003 (2003).
[22] N.F. Mott, J. Non-Cryst. Solids 1 (1968) 1.
[23] B.I. Shklovskii, A.L. Efros, Electronic Properties of Doped Semiconductors, Springer-Verlag, Berlin, 1984.